

Journal of Materials Chemistry B

Accepted Manuscript



This is an *Accepted Manuscript*, which has been through the Royal Society of Chemistry peer review process and has been accepted for publication.

Accepted Manuscripts are published online shortly after acceptance, before technical editing, formatting and proof reading. Using this free service, authors can make their results available to the community, in citable form, before we publish the edited article. We will replace this *Accepted Manuscript* with the edited and formatted *Advance Article* as soon as it is available.

You can find more information about *Accepted Manuscripts* in the [Information for Authors](#).

Please note that technical editing may introduce minor changes to the text and/or graphics, which may alter content. The journal's standard [Terms & Conditions](#) and the [Ethical guidelines](#) still apply. In no event shall the Royal Society of Chemistry be held responsible for any errors or omissions in this *Accepted Manuscript* or any consequences arising from the use of any information it contains.

Dual-functional carbon dots-silver@zinc oxide nanocomposite:***In vitro* evaluation of cellular uptake and apoptosis induction**

Abhay Sachdev^a, Ishita Matai^a and P.Gopinath^{*a,b}

^a*Nanobiotechnology Laboratory, Centre for Nanotechnology,*

^b*Department of Biotechnology,*

Indian Institute of Technology Roorkee, Roorkee, Uttarakhand-247667, India.

Fax: +91-1332-273560;

Tel: 91-1332-285650;

E-mail: pgopifnt@iitr.ernet.in, genegopi@gmail.com

Abstract

Carbon dots (CDs) are novel bioimaging tools with fascinating fluorescence properties. Herein, we report the development of novel carbon dots decorated silver-zinc oxide (CD-Ag@ZnO) nanocomposite (NC) consisting of highly fluorescent CDs and silver-zinc oxide (Ag@ZnO). The CD-Ag@ZnO NC was characterized by various analytical techniques. The article further provides an insight into the application of CD-Ag@ZnO NC in monitoring the cellular uptake and mediating apoptotic effects on MCF-7 and A549 cancer cells. By monitoring the simultaneous green fluorescence emission of CDs, the distribution of CD-Ag@ZnO NC was followed, eliminating the need of using fluorescent organic dyes. Fluorescence microscopy and atomic absorption spectroscopy (AAS) analyses were used for qualitative and quantitative assessment of cellular uptake. *In vitro* studies of CD-Ag@ZnO NC treated cancer cells revealed concentration dependent cytotoxic effects via induction of apoptosis. Fluorescence and scanning electron microscopy (SEM) were used to study the characteristic nuclear and morphological changes during apoptosis. We have used flow cytometry for quantifying the reactive oxygen species (ROS) and RT-PCR for studying the apoptotic gene expression. The role of ROS in eliciting the apoptotic gene cascade was also studied. Intriguingly, the multifunctional CD-Ag@ZnO NC has a tendency of evoking apoptosis meanwhile allowing the real-time intracellular trafficking, which can be of huge relevance for cancer theranostic applications.

Keywords: Carbon dots, Bioimaging, Nanocomposite, Apoptosis.

Introduction

Carbon dots (CDs) have raised high expectations in the field of biology owing to their intrinsic biocompatibility and remarkable fluorescence characteristics. Compared to conventional inorganic quantum dots, CDs can be prepared by simple chemical routes in a cost effective manner for bioimaging purposes^{1,2}. CDs have already proven their mettle for bioimaging of mammalian cells due their unique properties, such as water solubility, excitation-dependent multicolour emission, cell permeability, high cellular uptake and photostability³. The fluorescence properties and bioimaging efficiencies to a greater extent are influenced by surface functionality of CDs, as established by our previous report⁴. Conventionally, surface passivation is accomplished with the aid of several passivating agents and requires multiple time-consuming steps^{5,6}. The possibility of using PEG, a water soluble polymer, as a surface passivating agent for CDs has been explored recently by our group. This approach can evade the limitations associated with execution of surface passivation and produces brighter CDs with higher quantum yields in a single step^{4,7}. In the recent past, organic dyes have been incorporated into multifunctional nanocomposite (NC) systems for evaluating the cellular uptake. For example, coumarin-6 has been used as a fluorescent marker for evaluating the intracellular uptake of nanoparticles⁸⁻¹¹. However, coumarin-6 has certain disadvantages, such as water insolubility and cytotoxicity which discourages its use for intracellular studies. Alternatively, CDs possess the ability to circumvent the above issues and could be useful candidates for monitoring the cellular uptake. CDs based metal NCs is relatively new, yet exciting area of research since it renders the development of multifunctional materials with superior properties. Nevertheless, the luminescent property of CDs can be affected by metal nanoparticles, due to photoinduced electron transfer or aggregation of CDs¹²⁻¹⁴. Therefore, the challenge is to combine CDs with metal nanoparticles such that the NC has intact fluorescence properties. Besides, there have

been plenty of instances where metal-based nanocomposites (NCs) of CDs have been employed for biomedical ^{15,16}, catalytic ^{17,18}, surface enhanced raman spectroscopy (SERS) ¹⁴ and fluorescence based sensing ¹² applications. Over the recent years, metal based nanoparticles have been extensively applied for consumer- related applications. For instance, silver nanoparticles (Ag) are known for their antimicrobial action and have been used in bandages and water purifiers ^{19,20}. Similarly, zinc oxide nanoparticles (ZnO) have been employed in sunscreens ^{21,22}. On the other hand, silver-zinc oxide (Ag@ZnO) NC is also featured by their excellent antibacterial activity ²³. Thus, owing to increased exposure and widespread use of these nanoparticles, their cytotoxicity issues have been addressed in detail.

Lately, numerous studies have suggested the apoptosis inducing potential of Ag and ZnO nanoparticles. Characteristic morphological changes associated with apoptosis include membrane blebbing and cytoplasmic as well as nuclear constriction ^{24,25}. Further, Ag as well as ZnO has garnered a great deal of attention as potential apoptotic agents for anti-cancer therapy which has been confirmed through various mechanistic studies ²⁶⁻²⁸. However, most of the reported literatures did not give a clear idea about the cellular uptake of Ag and ZnO. Based on the above discussion, the combination of Ag@ZnO and CDs seems to be an ideal strategy for studying the intracellular uptake and apoptosis on cancer cells.

In the present work, an attempt has been made to combine CDs with Ag@ZnO to form CD-Ag@ZnO NC with dual functionality. We used PEG as a surface passivation agent for generating CDs in a one pot synthesis. It is expected that the negatively charged PEG passivation layer of CDs has the ability to form hybrid assembly with positively charged Ag@ZnO by electrostatic interaction. The rationale behind the study is to investigate the multifunctional aspects of CD-Ag@ZnO NC, exploiting the ability of Ag@ZnO component

to evoke apoptosis, while utilizing CDs as a fluorescence imaging probe simultaneously. To the best of our knowledge, this is the first instance involving the use of CDs for examining the cellular uptake of metal-based NC systems. MCF-7 (breast cancer) and A549 (lung cancer) cell lines were selected as model systems for the study since these are the most prevalent cancer types. Further, in order to elucidate the multiplex origin of apoptosis, levels of ROS were measured and apoptotic gene expression studies were performed.

Experimental Section

Materials

Chitosan and polyethylene glycol (PEG-4000) were purchased from Sisco Research Laboratories (SRL) Pvt. Ltd., India. Glacial acetic acid and citric acid were purchased from SD-fine chemicals limited (SDFCL), India. Zinc nitrate and silver nitrate were purchased from Himedia and Merck Pvt. Ltd., respectively. All the solutions were prepared in ultra pure water.

Synthesis of CDs

PEG passivated CDs (CD-PEG) were synthesized as described previously⁴. Briefly, 0.4 g of PEG-4000 was first dissolved uniformly in 60 mL of distilled water, followed by the addition of 300 μ L of acetic acid and 0.4 g of chitosan powder. The mixture was stirred vigorously for 30 min to form a homogenous solution. Then the solution was subjected to hydrothermal treatment at a constant temperature of 200°C for 8 h under nitrifying atmospheric conditions. Subsequently, the solution containing large, insoluble black precipitates was collected and centrifuged at 7400 g for 20 min. Finally, the supernatant containing yellow coloured CDs was obtained.

Synthesis of Ag@ZnO

The Ag@ZnO was synthesized according to a previous report²³. Equimolar amounts of Zinc nitrate and silver nitrate were added to 8% aqueous citric acid solution under stirring conditions. The transparent solution thus obtained was heated at 80 °C for 30 min. to form a gel. Microwave treatment of the obtained gel for 5–25 cycles (each cycle consists of 30 s on and 30 s off mode to prevent excessive boiling of the solvent) resulted in brownish fluffy solids. Then, the reaction product was washed with absolute ethanol and dried at 100 °C for 20 min. The resulting powder was further calcined at 500 °C for 2 h in a muffle furnace to obtain dark brown coloured Ag@ZnO nanopowder as the final product.

Synthesis of CD-Ag@ZnO NC

A stock solution of 1 mg/mL of Ag@ZnO was prepared in ultra pure water by sonicating for 15 min. Under continuous magnetic stirring, 500 µL aliquot of Ag@ZnO stock solution was mixed with 500 µL of aqueous solution of CDs (3 mg/mL). The reaction was allowed to proceed for 24 h at room temperature. Then, the product was centrifuged at 18000 g for 20 min to remove the excess, unreacted CDs. CD-Ag@ZnO NCs were collected as pellet and reconstituted to a final volume of 1mL in ultra pure water.

Characterization techniques

UV-vis and fluorescence spectra of the samples were recorded using a UV-vis double beam spectrophotometer (Lasany, LI-2800) and a fluorescence spectrophotometer (Hitachi F-4600, Japan). 20 µL of as-prepared sample was drop casted onto non-shining side of carbon-coated copper TEM grids and visualized by transmission electron microscope (TEM) (FEI TECHNAI G2) operating at 200 kV. The size analysis was performed through Image J software. A Fourier transform infrared (FTIR) spectrum of the NC was recorded on FTIR

spectrometer (Thermo Nicolet) in the range 4000–400 cm^{-1} using KBr disk-method. SEM-EDX analysis was carried out on field emission scanning electron microscope (FE-SEM) (QUANTA 200-FEG) and employed for elemental mapping to predict the elemental composition of the NCs. Fluorescence lifetimes were measured by a “Fluoro Cube Fluorescence Lifetime System” (Horiba Jobin Yvon) equipped with Nano LED (635 nm) source and decay curves were analysed by IBH decay analysis v 6.1 software. Various phases of the as-synthesized NC were studied by X-ray diffraction (XRD) and recorded using an advance powder X-ray diffractometer (Bruker AXS D8) by means of $\text{Cu-K}\alpha$ radiation, $\lambda = 1.5406 \text{ \AA}$, range of 0° – 90° at a scan rate of $0.05^\circ/\text{min}$ for 40 min. The zeta potential and size distribution of the samples in water (pH 7.0) were measured using Zetasizer (Malvern, Nano ZS 90). N_2 adsorption–desorption isotherms were obtained on a Quantachrome NOVA 2200e. The samples were degassed at 150°C for 2 h. The specific surface areas were determined from the adsorption data using the BET model and pore size was calculated by employing the BJH method. A fluorescent inverted microscope (EVOS[®] FL Color, AMEFC 4300) was used to acquire microscopic images of cells at various magnifications under bright field, DAPI (excitation 360 nm, emission 447 nm), GFP (excitation 470 nm, emission 525 nm) and RFP (excitation 530 nm, emission 593 nm) light cubes, respectively.

Cell culture

Several human cell lines used in this study, including A549 (human lung adenocarcinoma) cells, MCF-7 (breast adenocarcinoma) cells and L-132 (human normal lung epithelial) cells were procured from National Centre for Cell Sciences (NCCS), Pune, India. These cell lines were maintained in Dulbecco's modified Eagle's medium (DMEM, Sigma-Aldrich) supplemented with 10% (v/v) fetal bovine serum (FBS) and 1% penicillin-streptomycin solution (Sigma -Aldrich, USA) at 5% CO_2 in a humidified incubator at 37°C .

MTT assay

Cell viability was determined by measuring the mitochondrial activity of live cells to transform yellow colour MTT solution to a purple formazan product. Cells were seeded in 96-well tissue culture plates at a density of 10^4 cells/well and allowed to attach for 12 h. The cells were then incubated with medium containing different concentrations of CD-Ag@ZnO NC and Ag@ZnO for 12 h. After treatment, medium from each well was discarded and cells were washed once with phosphate buffer saline (PBS). Then, 100 μ L of fresh medium containing 10 μ L of MTT solution (5 mg/mL in PBS) was added to each well and incubated for another 4h. Medium containing MTT was aspirated and 150 μ L of DMSO was added to each well to dissolve the formazan crystals. Absorbance of each well was measured at 570 nm using a multi-mode microplate reader (Biotek, Cytation 3). The untreated cells (in DMEM) were used as control. Relative cell viability (mean% \pm SEM, n = 3) was calculated as:

$$\% \text{ Cell viability} = (\text{A}_{570} \text{ in treated sample} / \text{A}_{570} \text{ in control sample}) \times 100\%$$

In vitro cellular uptake

Cellular uptake was monitored qualitatively through fluorescence microscopy. Briefly, Cells were seeded on 6-well tissue culture plates at a density of 2×10^5 cells/ well. After 12h, different concentrations of the test samples were added to the wells. At the end of incubation, the medium was removed and cells were washed twice with PBS to remove the unbound samples. The cells were then observed under fluorescence microscope (EVOS[®] FL Color, AMEFC 4300). For quantitative determination of cellular uptake, 10^4 cells/well (100 μ L), were seeded in 96-well plate and incubated overnight for cell attachment. Different concentrations of CD-Ag@ZnO NCs were loaded in the wells and incubated for different periods of time. At the end of incubation, PBS wash was given twice to remove the unbound

dead cells. Next, 100 μL of 0.5% Triton X-100 in 0.2 M NaOH solution was added for cellular lysis. Multi-mode microplate reader (Biotek, Cytation 3) was used to quantify the fluorescence intensity from the released CD-Ag@ZnO NCs inside the wells at excitation and emission wavelengths of 320 nm and 400 nm, respectively.

Hoechst 33342 staining

Real time observation of nuclear uptake was monitored by incubating the MCF-7 and A549 cells in 6-well tissue culture plates with similar concentrations of CD-Ag@ZnO NCs for specified periods of time. After specific time spans, cells were stained with 3 μL of Hoechst 33342 (working concentration – 10 mg/mL) and incubated for 15 min. Finally, cells were given brief PBS wash and kept in PBS for imaging. An overlay of cell images was obtained by capturing images under blue and green filter of fluorescence microscope (EVOS[®] FL Color, AMEFC 4300).

Atomic absorption spectroscopy (AAS)

MCF-7 and A549 cells were seeded in 6-well tissue culture plates (2×10^5 cells/well) and exposed to different concentrations of CD-Ag@ZnO NCs, in duplicates, for 3 h. The cells were thoroughly washed and counted after exposure. Cells were then harvested by adding 1 mL of lysis solution (0.5% Triton X-100 in 0.2 M NaOH solution). Quantitative assessment of Ag and Zn uptake by A549 and MCF-7 cells was done by AAS in the graphite furnace mode (Avanta M, GBC Scientific Equipment). Calibration standards for Ag and Zn at concentrations of 2, 3, 4 ppm and 0.5, 1, 1.5 ppm were prepared from commercially available standards. Results were expressed as cellular dose of Ag/Zn in pg/cell.

Acridine Orange/Ethidium Bromide (AO/EB) staining

In order to distinguish between live, apoptotic and necrotic cells, the cells were stained with 10 μL of dual dye acridine orange/ethidium bromide (AO/EB) mixture (working concentration-10 $\mu\text{g}/\text{mL}$). Cells were grown in 6-well tissue culture plates and treated with different concentration of the test samples. After 6 h incubation, culture media was removed and cells were washed twice with PBS and stained with AO/EB in PBS. Stained overlay cell photographs were taken by capturing images under green and red filter of fluorescence microscope (EVOS[®] FL Color, AMEFC 4300).

Scanning electron microscopy (SEM)

For morphological analysis by SEM, 70%–80% confluent cells were grown on glass cover slip inside a 6-well tissue culture plate and were treated with CD-Ag@ZnO NCs for 6 h. The cells were then washed with PBS followed by fixation with 2% glutaraldehyde solution for 15 min. The fixed cells were then dehydrated by gradient ethanol solutions and air dried for examination by SEM.

Determination of reactive oxygen species (ROS)

MCF-7 and A549 cells were seeded in 6-well tissue culture plate (2×10^5 cells/well) were treated with varied concentrations of CD-Ag@ZnO and Ag@ZnO for 3 h. After twice PBS wash, 1 mL of DMEM containing 20 μM 2,7-dichlorofluorescein diacetate (DCFH-DA, Sigma Aldrich) dye was added and incubated for 15 min at 37°C. Immediately after the incubation, cells were trypsinized, collected and resuspended in PBS. Subsequently, samples were analyzed for the oxidized product, dichlorofluorescein (DCFH) fluorescence using flow cytometer (Amnis Flowsight) using 488 nm laser. Data analysis was performed on 10000

events per sample using Amnis Ideas software. Intracellular ROS production was reported in terms of percentage of cells with DCFH fluorescence.

Release of silver and zinc ions in DMEM

To examine the dissolution of CD-Ag@ZnO and Ag@ZnO in DMEM, the concentrations of silver and zinc ions released from CD-Ag@ZnO and Ag@ZnO after incubation at various time points were measured. At each time point, the samples were centrifuged at 14,000 g for 20 min and the supernatant was collected. Appropriate dilutions of the samples were digested with nitric acid (final concentration- 1%), prior to analysis. Finally, the resulting zinc and silver ion concentration was measured by AAS in the graphite furnace mode (Avanta M, GBC Scientific Equipment) using pure Ag (2, 3, 4 ppm) and pure Zn (0.5, 1, 1.5 ppm) standards as reference.

Semi-quantitative RT-PCR

For gene expression studies, MCF-7 cells (2×10^5 cells/well) were exposed to 50 $\mu\text{g}/\text{mL}$ of CD-Ag@ZnO NC for 5h. Afterwards, total RNA isolation was done using Tri reagent (Sigma Aldrich, USA) followed by reverse transcription (RT) of 1 μg of denatured RNA to generate cDNA. Gene expression was then studied using 1 μL of the above RT product using gene-specific forward and reverse primers in RT-PCR (Applied Biosystems). The cycling steps involved an initial denaturation at 94°C for 3min followed by PCR denaturation at 94°C for 30s, annealing at 60°C for 30s, extension at 72°C for 1min and final extension at 72°C for 10min. The amplified PCR products were finally resolved on ethidium bromide stained 1.2% agarose gel and visualized under UV light. The fold difference was computed using Image lab 4.0 software. The apoptotic genes selected for studying the expression included p53, caspase 3, bcl-xl. The housekeeping gene β actin was selected as internal control. The

forward and reverse primer sequences for all the primers used in the study are mentioned in Table S3 (Supporting information).

Statistical analysis

The data is expressed as mean \pm SEM of two or more individual experiments. The statistical data analysis was done by student's t test using GraphPad Prism 6.0. Statistically significant values are denoted by * ($p < 0.05$) and ** ($p < 0.001$).

Results and discussion

In the present study, we have demonstrated a simple method for synthesizing CD-Ag@ZnO NC by combining negatively charged CDs with positively charged Ag@ZnO through electrostatic interaction (Fig. 1(A)). The optical properties and formation of CD-Ag@ZnO NC was studied through various spectroscopic and microscopic techniques. The aqueous solutions of as-prepared CDs and Ag@ZnO depicted single absorption band at 257 nm ($\pi-\pi^*$ transition) and 372 nm, respectively, while CD-Ag@ZnO NC exhibited two absorption bands at 251 nm and 348 nm (Fig. 1(B)). On the other hand, the fluorescence intensity of CDs in CD-Ag@ZnO NC slightly decreased with respect to blank CDs (Fig. 1(C)). This could be due to photoinduced electron transfer between Ag@ZnO and CD components^{12,14}. Quantum yield of CD-Ag@ZnO NC was calculated to be 6.42%, which was comparable to that of CDs (6.74%) measured under similar parameters (Table S1). Similarly, fluorescence lifetime decay curves for CDs and CD-Ag@ZnO clearly show triple exponential decay and their average lifetimes were calculated (Fig. S1 and Table S2). Mean lifetime of CD-Ag@ZnO was estimated to be 5.035 ns, slightly less compared to CDs (5.204 ns). Further, the quantum yield and fluorescence lifetime measurements certify that Ag@ZnO did not completely quench the fluorescence of CDs in contrast to previous reports^{12,14}. This phenomenon appears to be

intimately linked with the electrostatic interactions between CD and Ag@ZnO, in contrast with covalent linkages which result in severe fluorescence quenching²⁹. Consequently, the electrostatic interactions of CDs to Ag@ZnO pursued in this work provides several advantages such as (i) the ability to retain the fluorescent properties without any reduction in quantum yield (ii) Minor reduction in fluorescence intensity of the NCs with respect to CDs suggests their potential for cell imaging²⁹. Transmission electron microscopy (TEM) image of CD-Ag@ZnO NC provides a direct evidence of the distribution of CDs on the surfaces of Ag@ZnO (Fig. 2(A)). The average size of the NC was estimated to be 37.5 ± 3.2 nm. Zeta potential measurements were done to examine the surface properties of CD-Ag@ZnO NC (Fig. 2(B)). The surface of CDs was negatively charged (zeta potential = -21.5 mV), while Ag@ZnO were positively charged (zeta potential= 22.3 mV). However, zeta potential of CD-Ag@ZnO NC was -10.8 mV which implied that Ag@ZnO were capped by CDs. As shown in Fig. 2(C), the average hydrodynamic diameter of CDs was 2.4 nm. After successful loading of CDs, the hydrodynamic diameter of CD-Ag@ZnO NC (39.58 nm) was slightly larger than the corresponding Ag@ZnO (34.16 nm). To further verify the presence of CDs and Ag@ZnO in the NC, elemental analysis was carried out using low magnification field emission-scanning electron microscope (FE-SEM) (Fig. 2(D)). Energy dispersive X-ray spectroscopy (EDS) elemental mapping distributions indicate the presence of C, Ag, Zn and O elements evenly distributed in CD-Ag@ZnO NC. The overlay SEM image further shows the presence of carbon on the surface, with the core consisting of Ag, Zn and O elements in agreement with the TEM and zeta potential measurements. Moreover, the EDAX spectrum revealed the relative percentage elemental composition of CD-Ag@ZnO NC as: 14.84% C, 56.11% Ag, 19.05% Zn and 10% O, respectively (Fig. S2). N₂ adsorption– desorption isotherms (Fig. S3) were recorded to ascertain the porous nature of Ag@ZnO. Calculations based on the adsorption data using the BJH model indicated that Ag@ZnO had a specific surface area of

6.560 m²/g, pore volume of 0.010 cm³/g and an average pore diameter of 1.49 nm. The TEM results (Fig. S4) depicts spherical that the CDs were mostly spherical averaging about 2.1 nm, which implies that CDs cannot penetrate the 1.49 nm pores of Ag@ZnO in CD-Ag@ZnO NC^{30,31}. The above observation is consistent with the TEM and zeta potential measurements. The phase structure of CD-Ag@ZnO NC was also explored. X-ray diffraction (XRD) pattern reveals a broad, amorphous peak at 22.63° which corresponds to (002) plane of CDs, while highly crystalline diffraction peaks match well with the typical Wurtzite ZnO (JCPDS card # 36-1451) and face centered cubic Ag (JCPDS card # 04-0783) phases, respectively (Fig. S5). Characteristic peaks obtained for CDs and Ag@ZnO are clearly in concurrence with the earlier reported literatures^{4,7,18,23}. Fourier transform infrared (FTIR) spectrum depicts specific functional groups present in CD-Ag@ZnO NC (Fig. S6). Peaks at 3432 cm⁻¹, 1638 cm⁻¹ and 1403 cm⁻¹ were due to O-H, C=O and C-N groups of CDs. Further, the passivating agent, PEG imparts O-H functionality to CDs^{4,7}. In addition, the peaks at 1090 cm⁻¹, 804 cm⁻¹ and 708 cm⁻¹ corresponded to Zn-O-Zn, Zn-O-H and Zn-O-Zn stretching frequencies and bending frequencies, respectively. Absorption bands at 476 cm⁻¹ and 652 cm⁻¹ were attributed to stretching vibrations of Zn-O and Ag-ZnO bonds²³. Notably, no C-Ag or C-Zn bonds were found. This indicated that negatively charged, O-H functionalized CDs were electrostatically adsorbed on the surface of Ag@ZnO component^{13,32}.

***In vitro* cytotoxicity**

The percentage of cell viability was determined quantitatively by MTT assay. MCF-7, A549 and L-132 cells were exposed to varying concentrations (10-90 µg/mL) of CD-Ag@ZnO NC. The obtained results show a significant reduction in viability of both the cancer cells in a dose-dependent manner. The IC₅₀ value (at which 50% cells are dead) of CD-Ag@ZnO against MCF-7 and A549 cells was found to be 50 µg/mL and 70 µg/mL, respectively (Fig.

3(A,B)). In contrast, blank Ag@ZnO treated MCF-7 and A549 cells exhibited severe decline in cell viability at similar concentrations. For example, the IC₅₀ value for Ag@ZnO treated MCF-7 and A549 cells was recorded to be 20 µg/mL and 50 µg/mL, which is far less compared to those estimated for CD-Ag@ZnO. However, CD-Ag@ZnO NC showed mild cytotoxicity towards normal L-132 cells compared to cancer cells in the same concentration range (Fig. 3(C)). To validate the same, the morphology of treated cells was examined by inverted microscope under bright field. A549 and MCF-7 cells treated with 50 µg/mL of CD-Ag@ZnO NC appeared rounded and shrunk in size. At similar concentration, treated L-132 cells showed predominantly healthy and normal morphology as that of untreated control cells with few rounded cells (Fig. S7). Moreover, the probable reason for lower cytotoxicity of CD-Ag@ZnO NC compared to blank Ag@ZnO could be due to the presence of CDs on the surface which prevents the premature interaction of the NC with the cells. Hence, the chances of aggregation of CD-Ag@ZnO NC in cell culture media are minimized, resulting in controlled cell death. Over and above, the biocompatibility of CDs was clearly established as cells treated with CDs had higher cell viability (nearly 97 %) even at a high concentration of 3 mg/mL compared to cells treated with CD-Ag@ZnO and Ag@ZnO (Fig. 3(D))⁴. By and large, these results indicate that the reduction in cell viability is primarily due to the action of Ag@ZnO component in CD-Ag@ZnO NC.

Cellular uptake

Cellular uptake is an important factor contributing to the action and cytotoxic effects of nanoparticles^{8,9,33,34}. MCF-7 and A549 cells were selected as models to evaluate the cellular uptake of CD-Ag@ZnO NC inside cancer cells. Cells were incubated with different concentrations of CD-Ag@ZnO NC and their uptake was monitored qualitatively by fluorescence microscope (Fig.4).The fluorescence emitted from CDs in CD-Ag@ZnO NC

was used to track its cellular localization. Blank CDs were internalized in the cytoplasm of the cells, but could not enter the nucleus (Fig. 4(e,m))⁴. However, in case of CD-Ag@ZnO NC treated cancer cells, cytoplasm as well as nuclear localization was observed in a dose-dependent manner. At lower concentration (20 $\mu\text{g/mL}$), CD-Ag@ZnO NCs were mostly distributed in the cytoplasm (Fig. 4(f,n)). Nevertheless, at higher concentrations (50 and 70 $\mu\text{g/mL}$), along with the cytoplasmic internalization, bright green fluorescence was also observed in the nucleus of MCF-7 and A549 cells (Fig. 4(g,h,o,p)). The plausible explanation for nuclear uptake could be the rupturing of nuclear membrane at higher concentrations, resulting in enhanced permeability to NC. Using Hoechst 33342 as a marker of nucleus, the cellular uptake of CD-Ag@ZnO NC was tracked^{30,35}. Onset of cellular uptake was observed after 0.5 h of treatment, followed by a continuous increase upto 3 h (Fig. 5). In both the cancer cell types, initially green fluorescence was observed around the cell nuclei. With the time-course, we observed colocalization of blue fluorescence (Hoechst 33342) with green fluorescence (CD-Ag@ZnO NC), suggesting nuclear internalization. Furthermore, cytoplasmic constriction was also observed with time. Furthermore, we used L-132 cells to examine the cellular uptake of CD-Ag@ZnO NC in normal cells. Interestingly, the normal cells exhibited efficient cellular uptake without any substantial cytotoxic effects at similar concentrations (Fig. S8)^{8,36}. However, no nuclear uptake was observed in normal cells, contrary to cancer cells. These results suggest differential uptake pattern of CD-Ag@ZnO NC on the human cancer and normal cells.

The cellular uptake of CD-Ag@ZnO NC was concentration and time-dependent (Fig. 6). As the concentration of NC increased, the fluorescence intensity and hence the uptake of NC increased in both MCF-7 and A549 cells (Fig. 6(A)). Likewise, enhanced uptake of CD-Ag@ZnO NC was observed with increasing incubation time till 3h in both the cancer cells (Fig. 6(B)). As evident from the above investigations, cellular uptake differed between the

two cancer cell lines. At equal concentrations and similar time points, CD-Ag@ZnO NCs were taken up by MCF-7 cells at higher levels than A549 cells. AAS was further used to quantify the cellular doses of Ag^+ and Zn^{2+} at different concentrations of CD-Ag@ZnO (Fig. 6(C,D))^{34,36}. Average Ag^+ concentration per cell was in the range of 6-10.4 pg for MCF-7 cells and 5.2-9.25 pg for A549 cells. Correspondingly, average Zn^{2+} content per cell was in the range of 4.67-12.39 pg (MCF-7) and 3.53-9.71 pg (A549). From the obtained results, it was apparent that MCF-7 cells had higher intracellular doses of Ag and Zn than A549 cells.

Cell death and cell morphology

Apoptosis inducing ability of Ag and ZnO is one of the widely studied mechanisms in cancer cells^{24-27,36-39}. To distinguish between live, apoptotic and necrotic cells in CD-Ag@ZnO NC treated MCF-7 and A549 cells, DNA intercalating acridine orange/ethidium bromide (AO/EB) dual dye staining was done^{24,25}. AO dye can permeate the cell nucleus of both viable and apoptotic cells and emits green fluorescence upon binding to double stranded DNA and red fluorescence when bound to single stranded DNA or RNA. Conversely, EB can only enter the cells with disrupted plasma membrane and emits orange fluorescence upon intercalating into DNA. Early apoptotic cells (EA) have intact cell membrane and show bright green granules indicating nuclear fragmentation. Late apoptotic cells (LA) have a compromised nuclear membrane with more permeability to EB and their nucleus appears orange in colour. The emission from CDs was not considered here because of the relatively weak fluorescence of bare CDs compared to fluorescent dye³⁰. As can be seen in Fig. 7(a,e), untreated MCF-7 and A549 cells appeared green indicating healthy viable cells. However, MCF-7 cells treated with lower concentration (20 $\mu\text{g}/\text{mL}$) of CD-Ag@ZnO NC displayed more number of EA and few LA cells (Fig. 7(b)), while only EA cells were seen at similar concentration in A549 cells (Fig. 7(f)). On the contrary, with increasing concentrations of NC

(50 and 70 $\mu\text{g/mL}$), LA cells were found to outnumber EA cells (Fig. 7(c,d,g,h)). FE-SEM studies were performed to study the morphological changes associated with apoptosis in CD-Ag@ZnO NC exposed cancer cells. Fig. 7(C) illustrated that control cells were spindle shaped, well-attached to the surface and had an intact membrane morphology. Contrarily, IC_{50} treated cells shrunk in size, became rounded, loosely- attached and exhibited membrane blebbing, which are the hallmarks of apoptotic cell death^{24,25}. Interestingly, the apoptotic effects of CD-Ag@ZnO NC were more pronounced in MCF-7 cells than A549 cells, clearly endorsing the higher cellular uptake of NC in MCF-7 cells.

ROS production and apoptotic genes expression

It is a well known fact that increased reactive oxygen species (ROS) levels can result in oxidative stress ultimately leading to apoptosis in cancer cells. Earlier studies have implicated excessive ROS production upon exposure to Ag as well as ZnO leading to cellular oxidative stresses^{24,25,27,36-39}. Under such circumstances, the efficiency of cellular antioxidant mechanisms gets reduced resulting in mitochondrial dysfunction and DNA damage^{8,33}. Therefore, in the present case, the role of oxidative stress in CD-Ag@ZnO NC mediated cytotoxicity was evaluated by 2',7'-dichlorodihydrofluorescein diacetate (DCFH-DA) dye based assay. This assay is based on the passive uptake of a non-fluorescent DCFH-DA dye, which reacts with ROS inside the cells and subsequently gets converted to highly fluorescent compound dichlorofluorescein (DCFH) by the action of intracellular esterases. The ROS levels were quantified by determining the percentage of fluorescent cells using a flow cytometer (Fig. 8). Herein, the fluorescent signal of CDs did not interfere much with the fluorescence signal of DCFH during flow measurements because of the relatively weak brightness of CDs compared to DCFH. From the results shown, it was clear that CD-Ag@ZnO NC treated cells showed more ROS production compared to untreated cells. For

MCF-7 treated cells, with an increase in the concentration of NC, the percentage of cells with elevated ROS increased from 14.4% to 47.6% accordingly (Fig. 8 (a-d)). Meanwhile, treated A549 cells also exhibited increased ROS generation in a dose dependent manner from 5.3% to 28% (Fig. 8(e-h)). At similar treatment concentrations, intracellular ROS production was found to be more in MCF-7 cells compared to A549 cells. For comparison, we also determined the percentage ROS induction in cancer cells treated with Ag@ZnO at identical concentrations. Intracellular ROS production increased from 24.1% to 81.6% for MCF-7 cells and 14.7% to 69.4% in A549 cells, respectively (Fig. S9), which is much higher compared to CD-Ag@ZnO treated cancer cells. The dissolution of Ag@ZnO and CD-Ag@ZnO NC in DMEM cell culture medium was analyzed by AAS (Fig. 9). Ag@ZnO released more Ag⁺ and Zn²⁺ ions than CD-Ag@ZnO NC at all lengths of time (3, 6 and 12 h) and at all concentrations (20, 50 and 70 ppm). Nevertheless, concentrations of ions released from the NC have been implicated for ROS production^{38,40}. Comparatively lower ROS production in CD-Ag@ZnO NC treated cancer cells was perhaps due to lesser release rate of Ag⁺ and Zn²⁺ ions from Ag@ZnO cores. Moreover, all the above findings perfectly correlate with the cytotoxicity and cellular uptake studies, wherein MCF-7 cells were found to be more sensitive than A549 cells under similar treatment regimes. Based on the above outcomes, it was favourable to use MCF-7 cells to explicate the apoptotic gene expression in CD-Ag@ZnO NC exposed cells with reference to untreated cells. In this regard, semiquantitative RT-PCR was used to analyze the expression levels of pro-apoptotic genes (p53, caspase 3, bax, bad, c-myc), anti-apoptotic genes (bcl-2, bcl-xl) and house-keeping gene (β actin) in MCF-7 cells. The results indicated up-regulation of p53, caspase 3, bax, bad, c-myc genes (indicated by upward arrow) and down-regulation of bcl-2, bcl-xl gene (indicated by downward arrow) in treated cells compared to untreated cells (Fig. 10(a,b)). Expression of β actin remained the same. It is already known that bcl-2 (B-cell lymphoma 2) family controls

the mitochondrial outer membrane permeabilization (MOMP) and could lead to pro-apoptotic (bax, bad) or anti-apoptotic effect (bcl-2, bcl-xl) by altering the inner mitochondrial membrane permeability transition pore⁴¹. Anti-apoptotic potential of bcl-xl (basal cell lymphoma-extra large) prevents the cell from entering into p53 mediated apoptosis. Further, destabilization of mitochondrial membrane by cytotoxic agents has been associated with caspase activation⁴¹. In our case, we observed the up-regulation of p53 gene which indicates the commencement of p53 mediated apoptotic pathway. Up-regulation of bax, bad along with down-regulation of bcl-2 and bcl-xl expression was also observed in cells treated with CD-Ag@ZnO NC which made the outer mitochondrial membrane more permeable. Additionally, p53 is known to up-regulate bax which is translocated to mitochondria and changes its membrane permeability⁴². This allows the secretion of cytochrome c into the cytosol leading to up-regulation of caspase 3 in treated cells, as observed in the present case^{43,44}. The above observations corroborate well with the previous reports^{24-28,37}. In succession, up-regulation of c-myc, a pro-apoptotic gene was also seen, which in turn plays a significant role in down-regulating anti-apoptotic genes, bcl-2 and bcl-xl. This is evident by increase in expression of c-myc together with decrease in expression of bcl-2 and bcl-xl genes.

Overall the sequence of events leading to apoptosis in CD-Ag@ZnO NC treated cells was illustrated. First, the NC attached and damaged the cell membrane integrity. Upon cellular uptake, the NC induced oxidative stress by evoking ROS and triggered the p53 mediated apoptotic pathway through which most of the chemotherapeutic drugs induce apoptosis (Fig. 10(c)).

Conclusion

In a nutshell, we have designed CD-Ag@ZnO NC simply by exploiting the electrostatic interactions between oppositely-charged CDs and Ag@ZnO. In this manner, the CDs in CD-

Ag@ZnO NC did not exhibit severe fluorescence quenching as suggested by spectroscopic studies. In addition, various characterization techniques (TEM, DLS, SEM) unanimously indicated that CDs successfully decorated the surface of Ag@ZnO to form a dual modality, hybrid assembly. Nonetheless, there are only a few studies on the development of CDs based NCs for biological applications. Most importantly, the proposed study provided sound evidence regarding the use of CD-Ag@ZnO NCs for inducing the apoptosis in cancer cells in conjugation with imaging. These NCs clearly demonstrated antiproliferative effects against both MCF-7 and A549 cancer cells in a dose dependent manner. Despite this potency, the CD-Ag@ZnO NC was less cytotoxic to normal lung L-132 cells than cancer cells in the same concentration range. Further, direct fluorescence monitoring of cellular uptake and intracellular localization of NC inside the cancer cells was also pursued using the fluorescence emission of CDs. Qualitative and quantitative analyses predicted marked differences in cellular uptake between MCF-7 and A549 cells. Preliminary investigation of apoptosis was done by dual dye staining and SEM analyses, which confirmed characteristic features of apoptosis like changes in the membrane permeability, morphology, cell shrinkage and cytoplasmic constriction in NC treated cancer cells. Moreover, a dramatic increase in ROS was observed in CD-Ag@ZnO NC treated cancer cells. Increased intracellular ROS production is associated with mitochondrial dysfunction ultimately leading to apoptosis. In this study, an increase in pro-apoptotic-to-anti-apoptotic expression ratio, activation of caspase 3 was observed in treated cancer cells. From these results, we demonstrated that CD-Ag@ZnO NC induced ROS-mediated activation of apoptotic gene signaling cascade consistent with the previous studies. Taken together, the implication of the present findings seems to be promising for the possible application of fluorescent CDs for theranostic purposes. Conversely, CDs can be used to distinguish between normal and apoptotic cells under fluorescence microscopy based on changes in the cell shape and morphology, adding a

new dimension to the use of CDs for apoptosis imaging. This work is further expected to motivate the development of specific tumor-targeted CDs in combination with metal nanoparticles/chemotherapeutic drugs for cancer theranostic applications.

Acknowledgement

Our sincere thanks to Science and Engineering Research Board (No. SR/FT/LS-57/2012) and Department of Biotechnology (No.BT/PR6804/GBD/27/486/2012), Government of India, for the financial support. Department of Chemistry and Institute Instrumentation Centre, Indian Institute of Technology Roorkee are sincerely acknowledged for providing various analytical facilities.

References:

1. H. Li, Z. Kang, Y. Liu and S-T. Lee, *J. Mater. Chem.*, 2012, **22**, 24230-24253.
2. S. N. Baker and G. A. Baker, *Angew. Chem. Int. Ed.*, 2010, **49**, 6726 – 6744.
3. P. G. Luo, S. Sahu, S.-T. Yang, S. K. Sonkar, J. Wang, H. Wang, G. E. LeCroy, L. Cao and Y-P. Sun, *J. Mater. Chem. B*, 2013, **1**, 2116–2127.
4. A. Sachdev, I. Matai and P. Gopinath, *RSC Adv.*, 2014, **4**, 20915-20921.
5. Y- P. Sun, B. Zhou, Y. Lin, W. Wang, K. A. S. Fernando, P. Pathak, M. J. Meziari, B. A. Harruff, X. Wang, H. F. Wang, P. J. G. Luo, H. Yang, M. E. Kose, B. L. Chen, L. M. Veca and S- Y Xie, *J. Am. Chem. Soc.*, 2006, **128**, 7756–7757.
6. H. Peng and J. Travas-Sejdic, *Chem. Mater.*, 2009, **21**, 5563–5565.
7. A. Sachdev, I. Matai, S. U. Kumar, B. Bhushan, P. Dubey and P. Gopinath, *RSC Adv.*, 2013, **3**, 16958-16961.
8. W. Liu, X. Li, Y.S. Wong, W. Zheng, Y. Zhang, W. Cao and T. Chen, *ACS Nano*, 2012, **6**, 6578-6591.

9. H. Gao, Z. Yang, S. Zhang, S. Cao, S. Shen, Z. Pang and X. Jiang, *Sci. Rep.*, 2013, **3**, 2534-2541.
10. W. Tao, X. Zeng, J. Zhang, H. Zhu, D. Chang, X. Zhang, Y. Gao, J. Tang, L. Huang and L. Mei, *Biomater. Sci.*, 2014, **2**, 1262-1274.
11. Y. Huang, L. He, W. Liu, C. Fan, W. Zheng, Y.S. Wong and T. Chen, *Biomaterials*, 2013, **34**, 7106-7016.
12. Q. Wang, H. Song, Y. Hu, Y. Su and Yi. Lv, *RSC Adv.*, 2014, **4**, 3992-3997.
13. J. Li, B. Zhang, F. Wang and C.Y. Liu, *New J. Chem.*, 2011, **35**, 554-557.
14. P. Luo, C. Li and G. Shi, *Phys. Chem. Chem. Phys.*, 2012, **14**, 7360-7366.
15. A. Kleinauskas, S. Rocha, S. Sahu, Y-P. Sun and P. Juzenas, *Nanotechnology*, 2013, **24**, 325103.
16. G-Y. Mao, W-J. Yang, F-X. Bu, D-M. Jiang, Z-J. Zhao, Q-H. Zhang, Q-C. Fang and J-S. Jiang, *J. Mater. Chem. B*, 2014, **2**, 4481-4488.
17. P. Mondal, K. Ghosal, S. K. Bhattacharyya, M. Das, A. Bera, D. Ganguly, P. Kumar, J. Dwivedi, R. K. Gupta, A. A. Martí, B. K. Gupta and S. Maiti, *RSC Adv.*, 2014, **4**, 25863-25866.
18. H. Yu, H. Zhang, H. Huang, Y. Liu, H. Li, H. Ming and Z. Kang, *New J. Chem.*, 2012, **36**, 1031-1035.
19. V. C. Mazurak, R. E. Burrell, E. E. Tredget, M. T. Clandinin and C. J. Field, *Burns*, 2007, **33**, 52-58.
20. T. A. Dankovich, *Environ. Sci.: Nano*, 2014, **1**, 367-378.
21. K. Schilling, B. Bradford, D. Castelli, E. Dufour, J.F. Nash, W. Pape, S. Schulte, I. Tooley, J. van den Bosch and F. Schellauf, *Photochem Photobiol Sci.*, 2010, **9**, 495-509.
22. T. G. Smijs and S. Pavel, *Nanotechnology, Science and Applications*, 2011, **4**, 95-112.

23. I. Matai, A. Sachdev, P. Dubey, S. U. Kumar, B. Bhushan and P. Gopinath, *Colloids Surf B Biointerfaces*, 2014, **115**, 359–367.
24. P. Sanpui, A. Chattopadhyay and S. S. Ghosh, *ACS Appl. Mater. Interfaces*, 2011, **3**, 218–228.
25. S. Sharma, S. Chockalingam, P. Sanpui, A. Chattopadhyay and S. S. Ghosh, *Adv. Healthcare Mater.* 2014, **3**, 106–114.
26. P. Gopinath, S. K. Gogoi, P. Sanpui, A. Paul, A. Chattopadhyay and S. S. Ghosh, *Colloids Surf B Biointerfaces*, 2010, **77**, 240–245.
27. R. Wahab, M.A. Siddiqui, Q. Saquib, S. Dwivedi, J. Ahmad, J. Musarrat, A. A. Al-Khedhairy and H-S. Shin, *Colloids Surf B Biointerfaces*, 2014, **117**, 267–276.
28. V. Sharma, D. Anderson and A. Dhawan, *Apoptosis*, 2012, **17**, 852–870.
29. K. K. R. Datta, O. Kozák, V. Ranc, M. Havrdová, A. B. Bourlinos, K. Šafářová, K. Holá, K. Tománková, G. Zoppellaro, M. Otyepka and R. Zbořil, *Chem. Commun.*, 2014, **50**, 10782-10785.
30. Q. Wang, X. Huang, Y. Long, X. Wang, H. Zhang, R. Zhu, L. Liang, P. Teng and H. Zheng, *Carbon*, 2013, **59**, 192–199.
31. L. Zhou, Z. Li, Z. Liu, J. Ren and X. Qu, *Langmuir*, 2013, **29**, 6396–6403.
32. J. Bian, C. Huang, L. Wang, T. Hung, W.A. Daoud and R. Zhang, *ACS Appl. Mater. Interfaces*, 2014, **6**, 4883-4890.
33. B. Yu, X. Li, W. Zheng, Y. Feng, Y-S.Wong and T. Chen, *J. Mater. Chem. B*, 2014, **2**, 5409-5418.
34. A.R. Gliga, S. Skoglund, I.O. Wallinder, B. Fadeel and H.L. Karlsson, *Part. Fibre Toxicol.*, 2014, **11**, 11-27.
35. M.X. Zhao, E-Z. Zeng, Y. Li and C-J. Wang, *J. Mater. Chem. B*, 2014, doi: 10.1039/C4TB01048E.

36. S. Mukherjee, D. Chowdhury, R. Kotcherlakota, S. Patra, B V, M.P. Bhadra, B. Sreedhar and C.R. Patra, *Theranostics*, 2014, **4**, 316-335.
37. M.J. Akhtar, M. Ahamed, S. Kumar, M.M. Khan, J. Ahmad and S.A. Alrokayan, *Int.J. Nanomedicine*, 2012, **7**, 845-857.
38. I.L. Hsiao and Y.J. Huang, *Chem. Res. Toxicol.*, 2011, **24**, 303–313.
39. J.W. Rasmussen, E. Martinez, P. Louka and D.G. Wingett, *Expert Opin Drug Deliv.*, 2010, **7**, 1063-1077.
40. T.W. Turney, M.B. Duriska, V. Jayaratne, A. Elbaz, S.J. O'Keefe, A.S. Hastings, T.J. Piva, P.F. Wright and B.N. Feltis, *Chem. Res. Toxicol.*, 2012, **25**, 2057–2066.
41. D.T. Chao and S.J. Korsmeyer, *Annu. Rev. Immunol.*, 1998, **16**, 395–419.
42. K.G. Wolter, Y. Hsu, C.L. Smith, A. Nechushtan, X. Xi and R.J.J. Youle, *Cell Biol.*, 1997, **139**, 1281-1292.
43. J. Yang, X. Liu, K. Bhalla, C.N. Kim, A.M. Ibrado, J. Cai, T.I. Peng, D.P. Jones and X. Wang, *Science*, 1997, **275**, 1129–1132.
44. R.M. Kluck, E. Wetzl-Bossy, D.R. Green, D.D. Newmeyer, *Science*, 1997, **275**, 1132–1136.

List of Figures

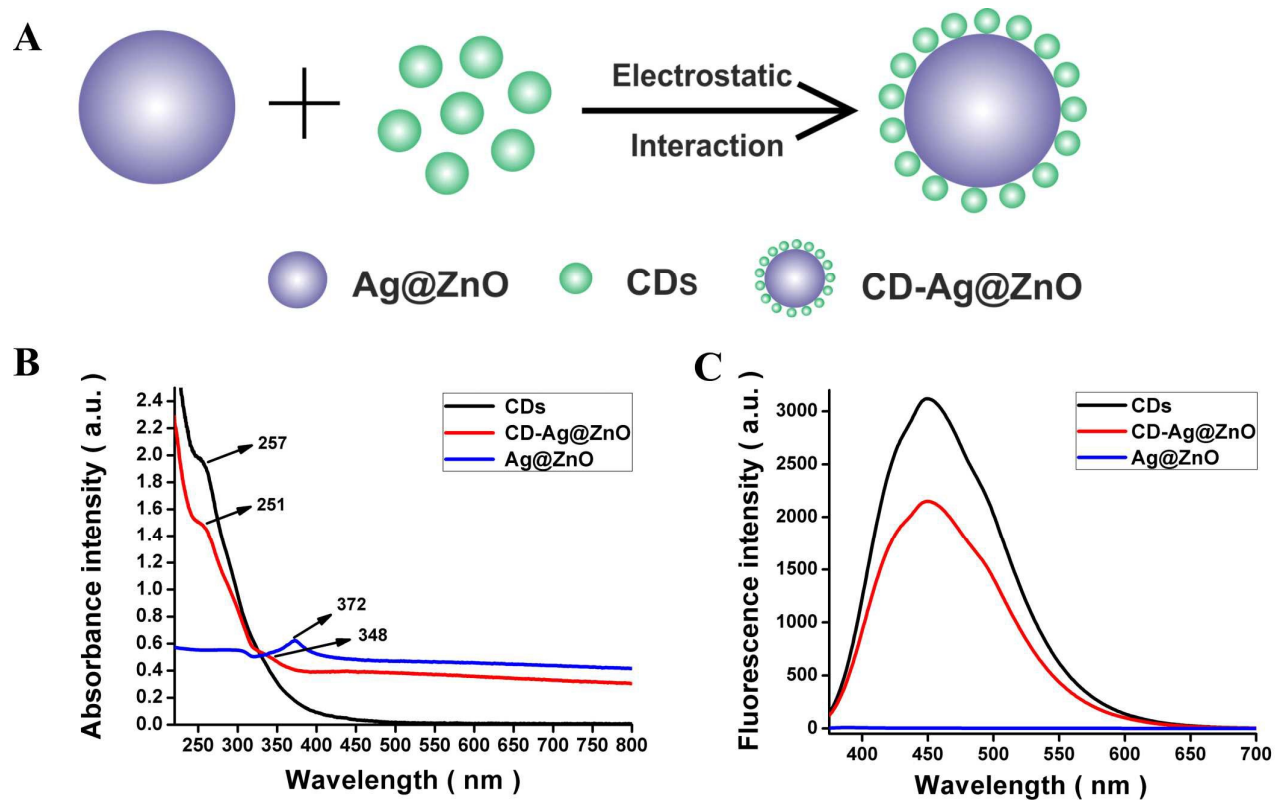


Fig.1 (A) Schematic illustration for synthesis of CD-Ag@ZnO NC. (B) UV-vis absorption spectra. (C) Fluorescence emission spectra ($\lambda_{\text{ex}} = 320 \text{ nm}$; $\lambda_{\text{em}} = 400 \text{ nm}$).

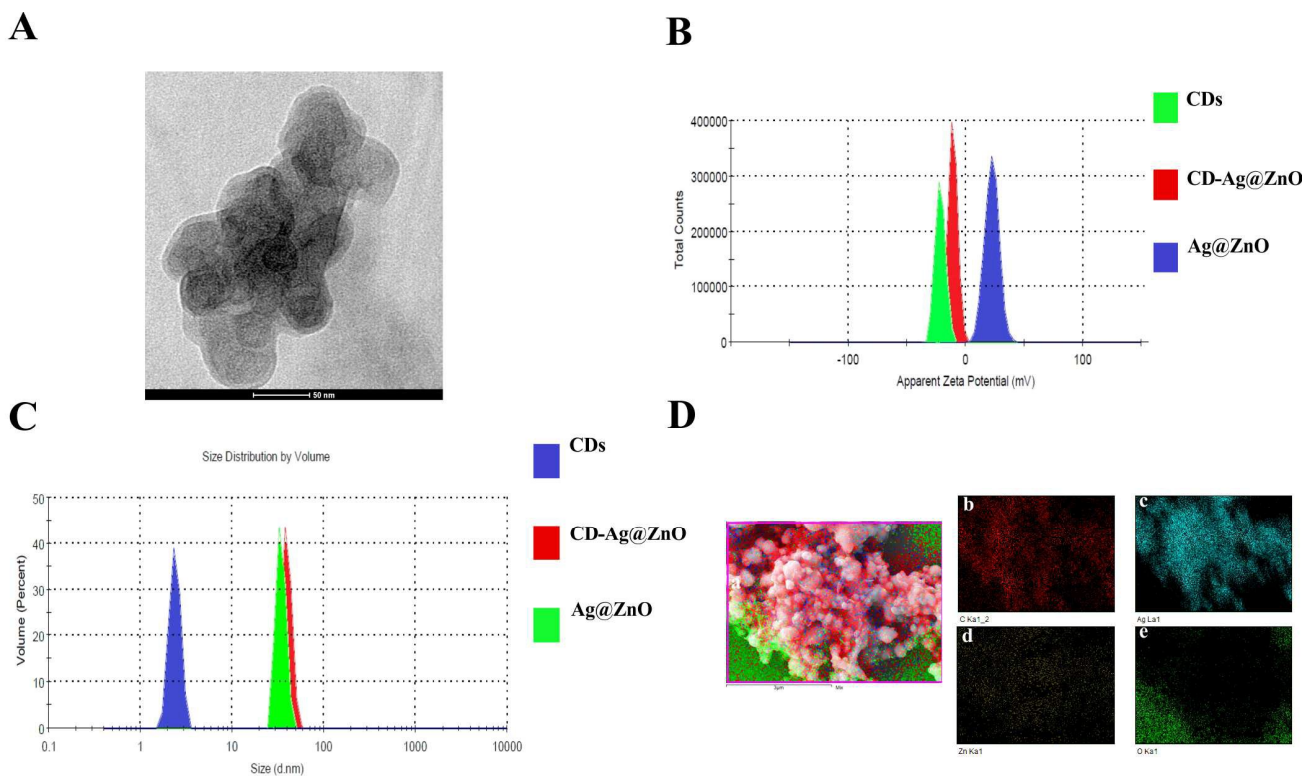


Fig. 2 (A) Representative TEM image of CD-Ag@ZnO NC. (B) Zeta potential, (C) Size distribution of aqueous solutions of CDs, CD-Ag@ZnO and Ag@ZnO at pH 7.0. (D) FE-SEM image of CD-Ag@ZnO NC and colour coded SEM/EDX dot maps. (a) Overlay FE-SEM image depicting elemental distributions in CD-Ag@ZnO NC. (b-e) Individual elemental distribution (red for carbon, cyan for silver, yellow for zinc and green for oxygen).

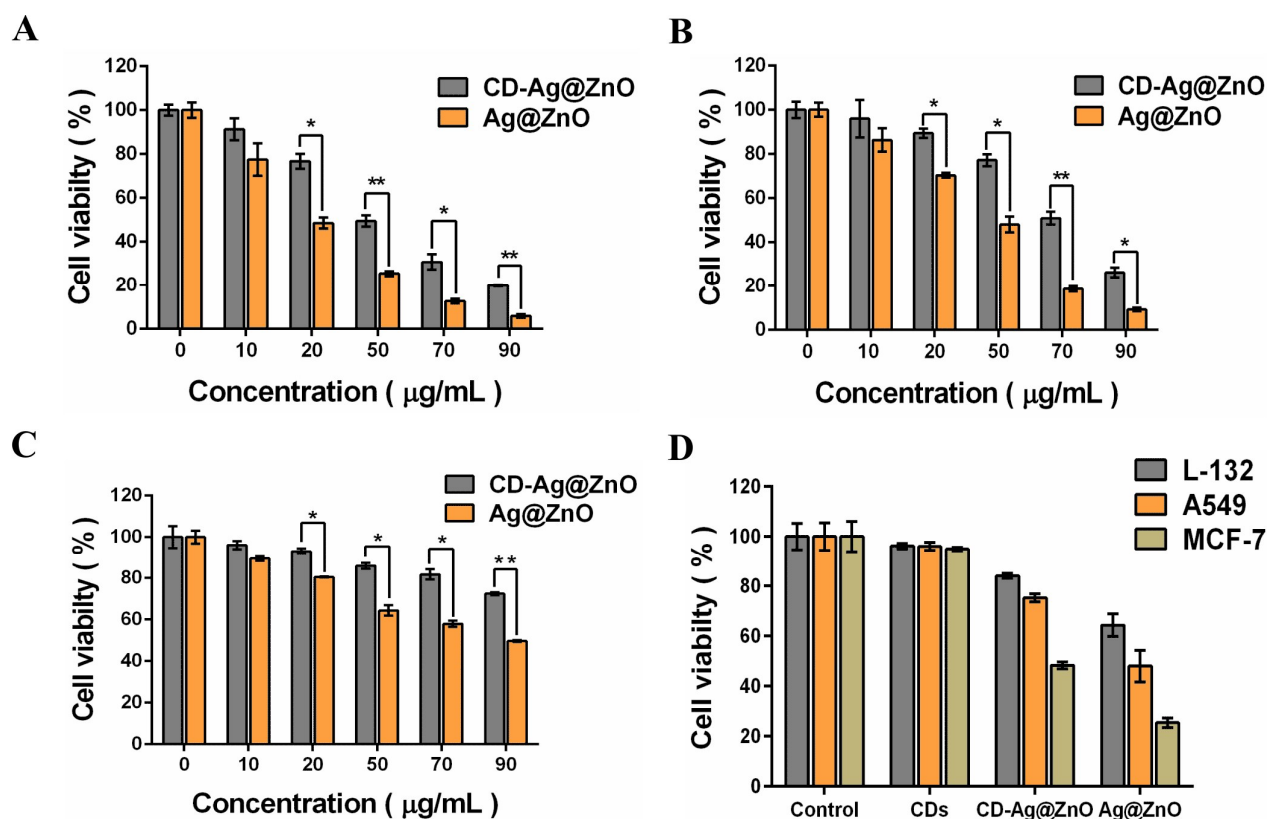


Fig. 3 Cell viability of (A) MCF-7 (B) A549 and (C) L-132 cells as estimated from the MTT assay. (D) Comparative cytotoxicity analysis of CDs (3mg/mL), CD-Ag@ZnO (50 μg/mL) and Ag@ZnO (50 μg/mL). The values are represented as mean ± S.E.M. of three individual experiments. Statistical significance between samples treated with CD-Ag@ZnO NC and blank Ag@ZnO is denoted by * ($p < 0.05$) and ** ($p < 0.001$).

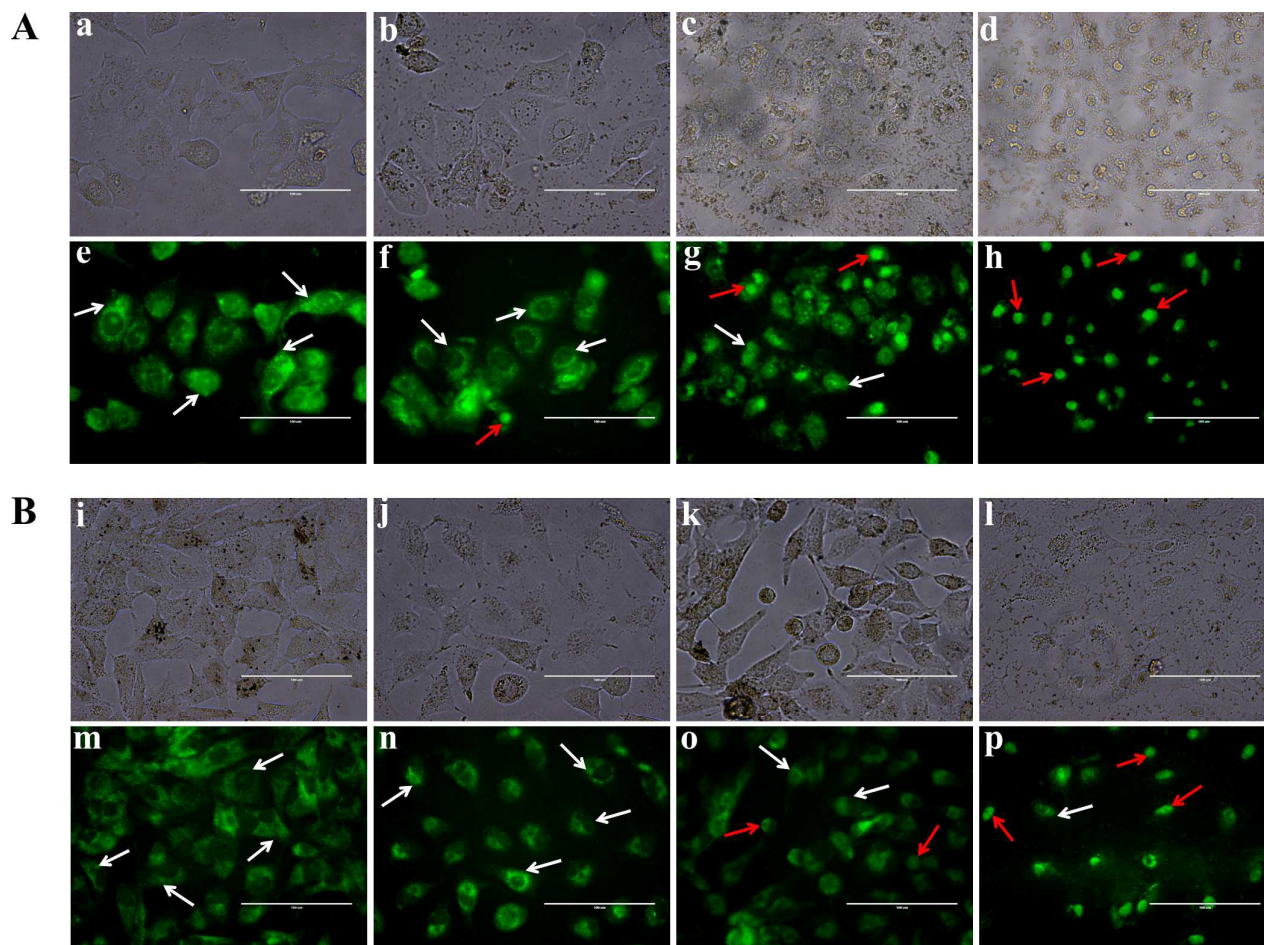


Fig. 4 Fluorescence microscopic images depicting the cellular uptake in (A) MCF-7 and (B) A549 cells. Upper panel: a,e) CDs and b,f) 20 $\mu\text{g/mL}$, c,g) 50 $\mu\text{g/mL}$, d,h) 70 $\mu\text{g/mL}$ CD-Ag@ZnO NC treated MCF-7 cells. Lower panel: i,m) CDs and j,n) 20 $\mu\text{g/mL}$, k,o) 50 $\mu\text{g/mL}$, l,p) 70 $\mu\text{g/mL}$ CD-Ag@ZnO NC treated A549 cells. The images in the (a–d) and (i–l) are corresponding bright field images. White and Red arrows represent cytoplasm and nuclear localization, respectively. Scale bar: 100 μm .

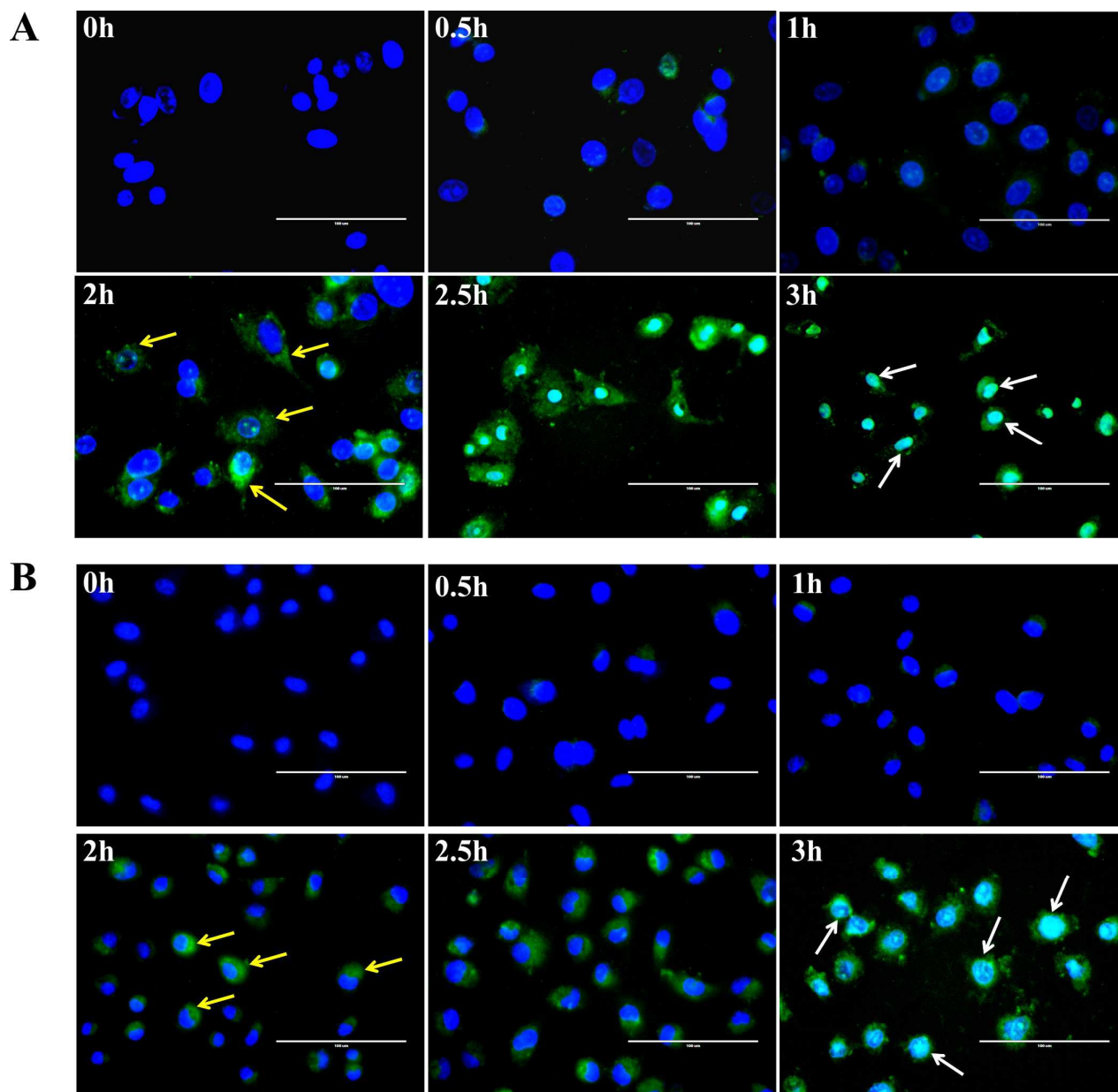


Fig. 5 Time –dependent overlay images of (A) MCF-7 and (B) A549 cells treated with 50μg/mL CD-Ag@ZnO NC and stained with Hoechst 33342. Yellow and white arrows represent cytoplasm and nuclear localization, respectively. Overlay images have been acquired using a combination of DAPI (for Hoechst 33342) and GFP (for CD-Ag@ZnO NC) filters. Scale bar: 100 μm.

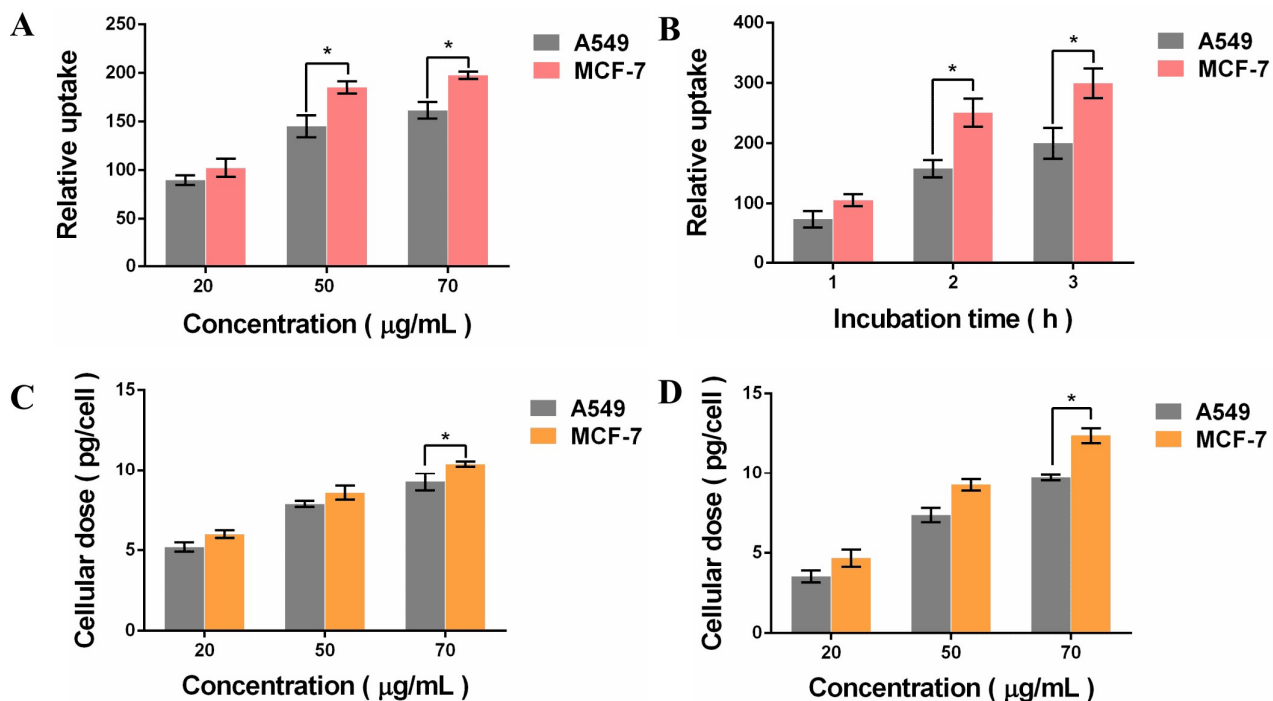


Fig.6 Quantitative cellular uptake of CD-Ag@ZnO NC.(A) Cellular uptake of different concentrations of CD-Ag@ZnO NC for 2h (B) Cellular uptake of 50 µg/mL CD-Ag@ZnO NC for different times. Quantitative cellular doses of (C) Ag and (D) Zn treated with different concentrations of CD-Ag@ZnO NC for 3h. The values are represented as mean \pm S.E.M. of two individual experiments. Statistical significance between MCF-7 and A549 cells treated with CD-Ag@ZnO NC is denoted by * ($p < 0.05$).

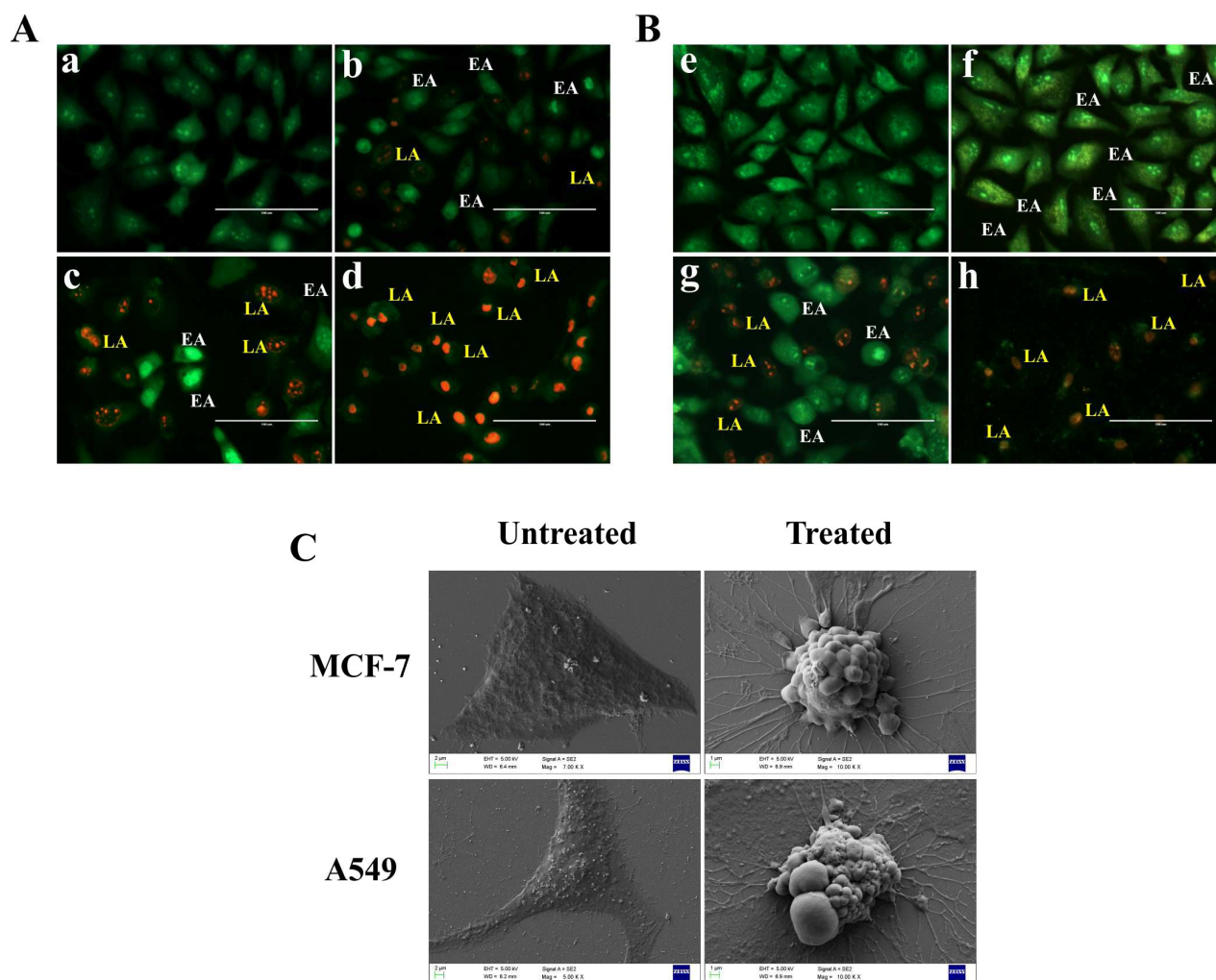


Fig. 7 Fluorescence microscopic images of AO/EB stained cells of (A) MCF-7 and (B) A549 cells. (a,e) untreated and (b,f) 20 $\mu\text{g/mL}$, (c,g) 50 $\mu\text{g/mL}$, (d,h) 70 $\mu\text{g/mL}$ CD-Ag@ZnO NC treated cells. EA and LA represent early apoptotic and late apoptotic cells, respectively. Scale bar: 100 μm . (C) Representative SEM images of untreated and CD-Ag@ZnO NC treated cells. Scale bar: 2 μm (untreated) and 1 μm (treated).

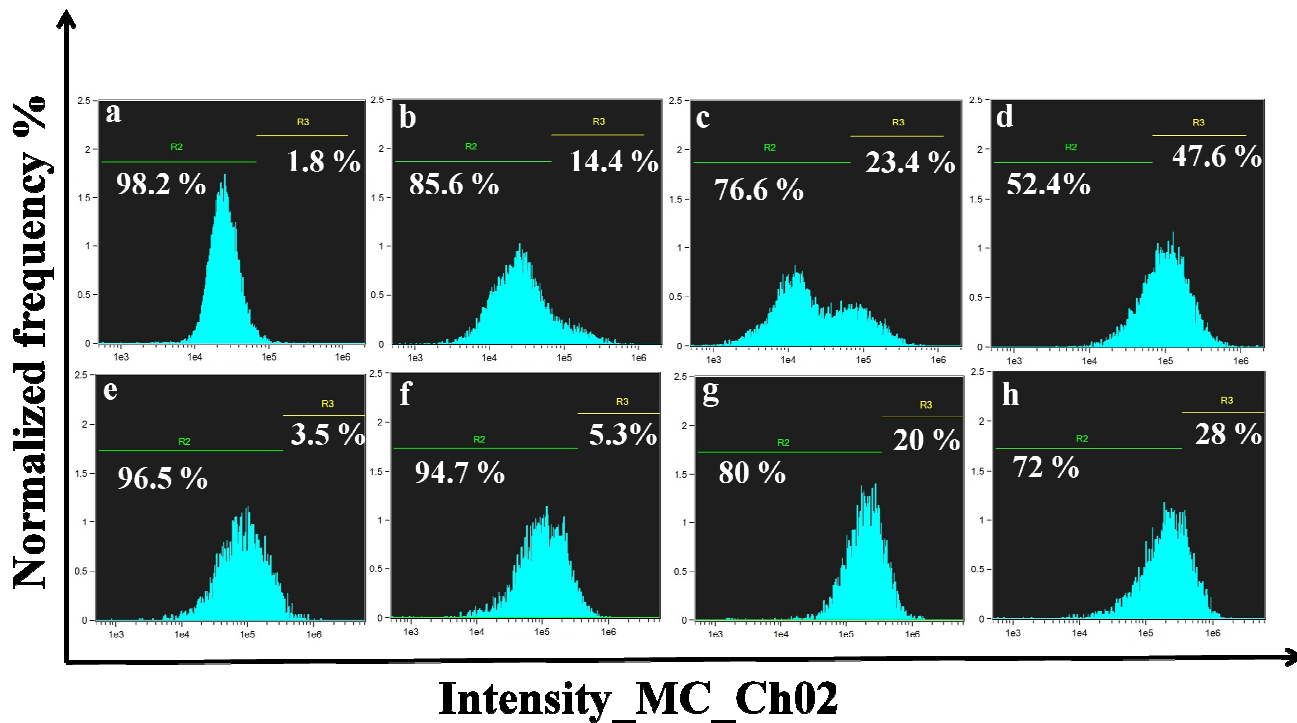


Fig. 8 Flow cytometric analysis of ROS production in MCF-7 and A549 cells. Upper panel: (a) untreated and (b) 20 $\mu\text{g/mL}$, (c) 50 $\mu\text{g/mL}$, (d) 70 $\mu\text{g/mL}$ CD-Ag@ZnO NC treated MCF-7 cells. Lower panel: (e) untreated and (f) 20 $\mu\text{g/mL}$, (g) 50 $\mu\text{g/mL}$, (h) 70 $\mu\text{g/mL}$ CD-Ag@ZnO NC treated A549 cells.

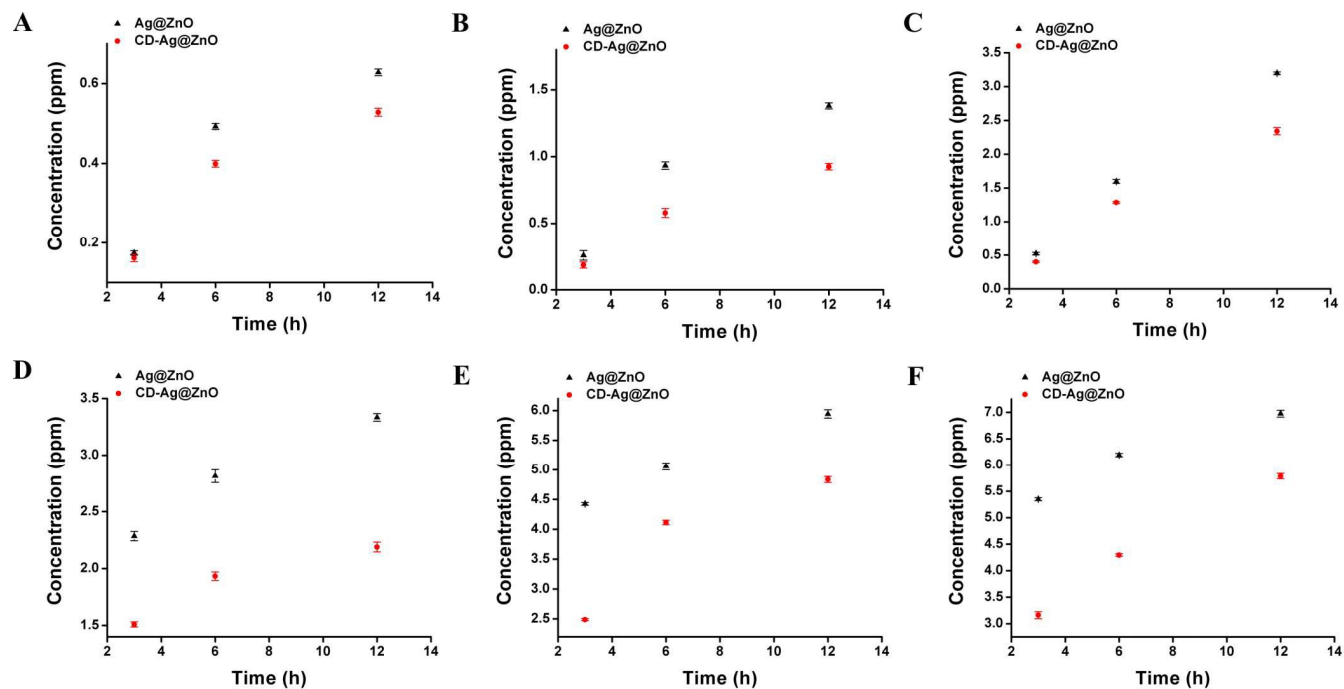


Fig. 9 AAS analyses of silver (A-C) and zinc (D-F) ions released from Ag@ZnO and CD-Ag@ZnO NC after 3, 6, and 12 h in DMEM. Particle suspension: (A,D) 20 ppm; (B,E) 50 ppm; (C,F) 70 ppm.

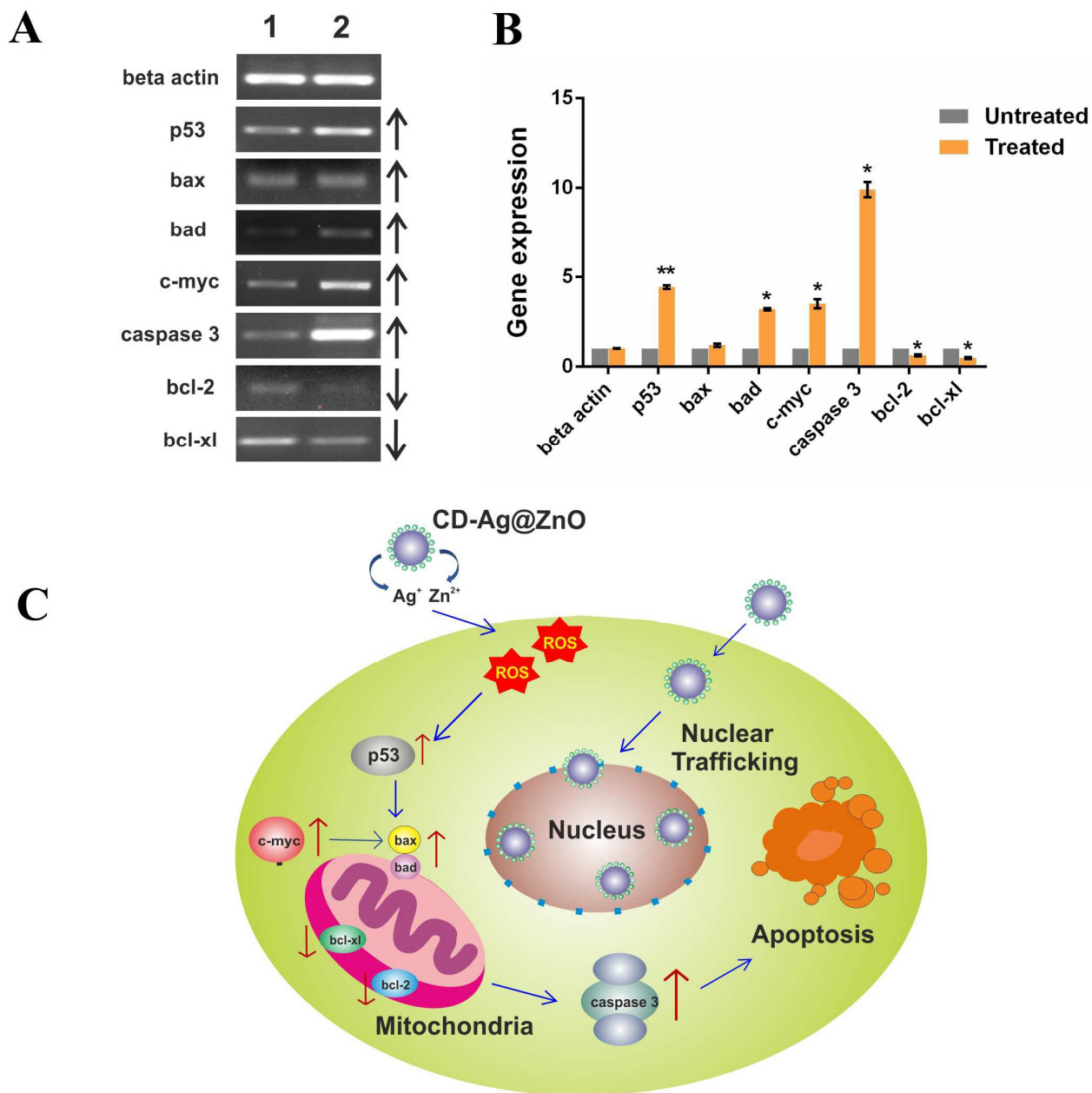


Fig. 10 (A) Semi-quantitative RT-PCR analysis of apoptotic signaling genes. Lane 1 and 2: untreated and CD-Ag@ZnO NC treated MCF-7 cells (50 $\mu\text{g}/\text{mL}$) respectively. (B) Fold difference in gene expression in treated MCF-7 cells as compared to untreated MCF-7 cells. Data is represented as mean \pm SD of two individual experiments. Statistical significance between groups is denoted by * ($p < 0.05$) and ** ($p < 0.001$). (C) Schematic illustration of cellular uptake and apoptosis induction by CD-Ag@ZnO NC.

Graphical abstract

Dual-functional carbon dots-silver@ zinc oxide nanocomposite:

In vitro evaluation of cellular uptake and apoptosis induction

Abhay Sachdev^a, Ishita Matai^a and P.Gopinath^{*a,b}

^a*Nanobiotechnology Laboratory, Centre for Nanotechnology,*

^b*Department of Biotechnology,*

Indian Institute of Technology Roorkee, Roorkee, Uttarakhand-247667, India.

Fax: +91-1332-273560;

Tel: 91-1332-285650;

E-mail: pgopifnt@iitr.ernet.in, genegopi@gmail.com

